Chemical Senses, 2019, Vol 44, 673–682
doi:10.1093/chemse/bjz062
Original Article
Advance Access publication 31 August 2019

Original Article

Optimization of Insect Odorant Receptor Trafficking and Functional Expression Via Transient Transfection in HEK293 Cells

Fabio Miazzi[1,2], Carolin Hoyer[1], Silke Sachse[1], Markus Knaden[1], Dieter Wicher[1], Bill S. Hansson[1*] and Sofia Lavista-Llanos[1*]

[1]Department of Evolutionary Neuroethology, Max Planck Institute for Chemical Ecology, Hans-Knöll-Str. 8, 07745, Jena, Germany and [2]Present address: Max Planck Institute for Chemical Ecology, Max Planck Research Group Predators and Toxic Prey, Hans-Knöll-Str. 8, 07745, Jena, Germany

Correspondence to be sent to: Fabio Miazzi, Max Planck Institute for Chemical Ecology, Max Planck Research Group Predators and Toxic Prey, Hans-Knöll-Str. 8, 07745, Jena, Germany. E-mail: fmiazzi@ice.mpg.de

*These authors share seniority.

Editorial Decision 28 August 2019.

Abstract

Insect odorant receptors (ORs) show a limited functional expression in various heterologous expression systems including insect and mammalian cells. This may be in part due to the absence of key components driving the release of these proteins from the endoplasmic reticulum and directing them to the plasma membrane. In order to mitigate this problem, we took advantage of small export signals within the human HCN1 and Rhodopsin that have been shown to promote protein release from the endoplasmic reticulum and the trafficking of post-Golgi vesicles, respectively. Moreover, we designed a new vector based on a bidirectional expression cassette to drive the functional expression of the insect odorant receptor coreceptor (Orco) and an odor-binding OR, simultaneously. We show that this new method can be used to reliably express insect ORs in HEK293 cells via transient transfection and that is highly suitable for downstream applications using automated and high-throughput imaging platforms.

Key words: *Drosophila melanogaster*, HCN1, odorant receptors, rhodopsin

Introduction

Insect odorant receptors (ORs) are 7 transmembrane-domain proteins, with an inverted topology compared to G protein-coupled receptors (GPCRs) (Benton et al. 2006; Butterwick et al. 2018), responsible for the detection of a vast number of chemically diverse odorants including pheromones (Hallem and Carlson 2006; Touhara and Vosshall 2009). They form heteromeric cation channels, constituted by an odor-binding receptor (OrX) and a highly conserved coreceptor named Orco (Krieger et al. 2003; Jones et al. 2005; Neuhaus et al. 2005; Benton et al. 2006; Sato et al. 2008; Wicher et al. 2008; Vosshall and Hansson 2011).

Several methods have been used to express insect ORs in heterologous systems in order to characterize their ligand specificity and to study their functional properties (Fleischer et al. 2018). For example, the so-called "empty neuron system" allows the ectopic expression of ORs in subsets of olfactory sensory neurons of the vinegar fly *Drosophila melanogaster* lacking the endogenous OrX, but with a fully functional Orco (Dobritsa et al. 2003; Kurtovic et al. 2007; Gonzalez et al. 2016). Moreover, in vitro expression systems allow the heterologous expression of OR proteins in animal cells including—among others—*Xenopus* oocytes (Nakagawa et al. 2005; Wang et al. 2010; Nakagawa and Touhara 2013), insect cells (Kiely

et al. 2007; Tsitoura et al. 2010; German et al. 2013), and mammalian cells (e.g., HEK293 and CHO) using vectors for transient expression (Sato et al. 2008; Wicher et al. 2008) or as stable lines (Grosse-Wilde et al. 2006; Jones et al. 2011; Corcoran et al. 2014).

Each of these methods offers several advantages, but also bears disadvantages: the "empty neuron system" allows the expression of OR proteins in an environment that is very similar to their native olfactory sensillum. However, the generation of transgenic fly lines and the electrophysiological recording tests can be time consuming and are not suitable for high-throughput screening experiments. *Xenopus* oocytes have been successfully used for extensive screenings of odors and are compatible with automated platforms, but the costs associated with *Xenopus* rearing or the purchase of oocytes can be prohibitive for very large screenings. Stable and inducible cell lines, on the other hand, originate from cell clones that successfully integrated in their genome an expression cassette containing a tetracycline-dependent promoter driving the expression of Orco and an odor-binding OrX. Such system represents a sort of "gold standard" as cell variability is strongly reduced, compared to transiently transfected cells, by selection of monoclonal populations and non-induced cells constitute an optimal internal negative control. Moreover, the selection of a monoclonal cell population represents—to date—the most effective approach to deal with the limited functional expression of ORs in the plasma membrane in heterologous systems due to an impaired intracellular trafficking of ORs both in insect (German et al. 2013) and mammalian cells (Halty-deLeon et al. 2016).

Although a thorough investigation of the bottlenecks in insect OR intracellular trafficking has not been performed yet, their retention within intracellular membranes (German et al. 2013) may be due to the lack of specialized components of the OR release mechanism from the endoplasmic reticulum (ER) and the Golgi apparatus in heterologous systems. Several membrane proteins have been shown to direct their intracellular trafficking through small peptide regions. Among others (Schülein et al. 1998; Ammon et al. 2002), it has been shown that an N-terminal peptide (^{106}VNKFSL^{111}) from the human HCN1 channel facilitates the exit of HCN1 proteins from the ER (Pan et al. 2015), and the C-terminal portion of the human Rhodopsin (^{344}QVAPA^{348})—containing the "VxPx" motif—is sufficient to promote the formation of post-Golgi vesicles and their trafficking to the plasma membrane via microtubule-mediated transport (Tai et al. 1999; Deretic et al. 2005; Mazelova et al. 2009; Lodowski et al. 2013).

In this work, we investigated whether insect ORs tagged at their N-terminus with the HCN1 and Rhodopsin signal peptides show an enhanced trafficking to the plasma membrane in mammalian cells and reach satisfactory functional expression levels even after transient transfection without clonal selection. Moreover, in order to increase the efficiency of gene cotransfection, we designed a new vector based on a commercially available dual-promoter plasmid for mammalian transient transfection. In this way, we aimed at creating a new fast and inexpensive strategy to reliably express insect ORs in mammalian cells for a broad range of application, including automated and high-throughput imaging systems.

Materials and methods

Constructs

A human codon-optimized version of *D. melanogaster* Or47a (hOr47a) tagged at the N-terminus with the peptide "QVAPAGKPIPNPLLGLDSTVNKFSL" coding for the human Rhodopsin ^{344}QVAPA^{348} peptide (minimal Rho tag, abbreviated as "mRho" or "R" tag), a V5 tag (GKPIPNPLLGLDST) and the human HCN1 peptide ^{106}VNKFSL^{111} (minimal ER export tag, abbreviated as "mER" or "E" tag)—this construct is hereafter called mRho.V5.mER.hOr47a, or R.E.hOr47a—was synthesized and subcloned into the pcDNA3.1(-) vector (Cat. Nr. V79520, Invitrogen) using the XbaI and XhoI restriction sites by Eurofins Genomics GmbH. Constructs bearing only the V5 and mER peptides (V5.mER.hOr47a, or abbreviated E.hOr47a) and the V5 tag only (V5.hOr47a, or abbreviated hOr47a) were obtained from the mRho.V5.mER.hOr47a construct via PCR using the Advantage 2 PCR kit (Cat. Nr. 639206, Takara) using the E.hOr47a_fwd and hOr47a_fwd forward primers, and the common (E.)hOr47a_rev reverse primer, respectively. A previously described nonhuman codon optimized version of *D. melanogaster* Orco cloned in pcDNA3.1(-) (Mukunda et al. 2014) was used for cotransfection of the hOr47a constructs in pcDNA3.1(-).

We created a high-copy number bidirectional expression vector (hence called pCMV-BI) by inserting the bidirectional promoter cassette flanked by the termination regions of the pBI-CMV1 vector (Cat. Nr. 631630, Clontech), in the pCMVTNT (Cat. Nr. L5620, Promega) vector backbone. Both regions were amplified using Phusion high-fidelity polymerase (Cat. Nr. M0530, New England Biolabs) with the pBI-CMV1_fwd, pBI-CMV1_rev, and pCMVTNT_fwd, pCMVTNT_rev primer couples, respectively. Fragments were assembled using the NEBuilder HiFi DNA Assembly Master Mix (Cat. Nr. E2621, New England Biolabs).

A human codon-optimized version of *D. melanogaster* Orco (hOrco) tagged at the N-terminus with a myc tag (5′-GAACAGAAA CTGATCTCTGAAGAAGACCTG-3′) was synthesized by Eurofins Genomics GmbH and subcloned into the pCMV-BI vector using the BamHI and HindIII restriction sites. A version of hOrco bearing the β-globin/IgG chimeric intron from the pCMVTNT vector within the hOrco sixth transmembrane domain was constructed by Phusion polymerase amplification using the hOrcoExon1_fwd, hOrcoExon1_rev, chimeric_intron_fwd, chimeric_intron_rev, hOrcoExon2_fwd and hOrcoExon2_rev primers. A new vector called pDmelOR was then created by cloning this intron-containing version of hOrco into the pCMV-BI vector, after digestion with BamHI and HindIII, using the NEBuilder HiFi DNA Assembly kit.

The mRho.V5.mER.hOr47a construct was inserted in the pDmelOR vector after linearization with EcoRI, using the BI-R.E.hOr47a_fwd and BI-R.E.hOr47a_rev using the NEBuilder HiFi DNA Assembly Master Mix (pDmelOR-mRho.V5.mER.hOr47a, or pDmelOR-R.E.hOr47a). Moreover, a human codon-optimized version of *D. melanogaster* Or56a (hOr56a) was synthesized by Eurofins Genomics GmbH and inserted in the pDmelOR vector after linearization with EcoRI, together with the mRho.V5.mER tag using the following set of primers: hOr56a_fwd, hOr56a_rev, hOr56aTag_fwd, hOr56aTag_rev (pDmelOR-mRho.V5.mER.hOr56a, or pDmelOR-R.E.hOr56a).

All sequences were verified by Sanger sequencing (by Eurofins Genomics GmbH and the Department of Entomology, Max Planck Institute for Chemical Ecology, Jena). The CMV enhancer region of the pCMV-BI empty plasmid was sequenced using the pBI-CAG_for and pBI-CAG_rev primers. Sequencing of CMV promoter and termination regions from pCMV-BI and related constructs required a preliminary digestion with restriction enzymes, band isolation and purification after gel electrophoresis and possibly amplification of target sequences due to the presence of 2 very similar CMV promoter and SV40 polyA regions. The pCMV-BI empty plasmid was

digested with DraIII-HF (Cat. Nr. R3510, New England Biolabs) and NcoI-HF (Cat. Nr. R3193, New England Biolabs). The pDmelOR vector was sequenced after digestion with XhoI and PvuI-HF (Cat. Nr. R3150, New England Biolabs); constructs with inserted Or47a and Or56a genes were cut with XhoI and NaeI (Cat. Nr. R0190, New England Biolabs). If required, the inserted Orco gene was subsequently amplified from the Orco-bearing purified plasmid fragment with the pBI-Orco_for and pBI-Orco_rev primers, and the tuning receptor gene with the pBI-OrX_fwd, pBI-OrX_rev primers using the Advantage 2 PCR kit and the resulting PCR products were sequenced. Primer sequences are listed in the Supplementary Table 1

Full sequences for the reported constructs and plasmid availability information are accessible at Addgene (https://www.addgene.org) with the following reference numbers: pcDNA3.1(-)-mRho.V5.mER.hOr47a: #126472; pcDNA3.1(-)-V5.mER.hOr47a: #126473; pcDNA3.1(-)-V5.hOr47a: #126474; pCMV-BI: #126475; pDmelOR: #126476; pDmelOR-mRho.V5.mER.hOr47a: #126478; pDmelOR-mRho.V5.mER.hOr56a: #126479.

Transient expression in mammalian cells

HEK293 cells (DSMZ no. ACC 305) were purchased from the Leibniz Institute DSMZ GmbH and grown in DMEM/F12 1:1 medium (Cat. Nr. 11320, Gibco, Life Technologies) supplied with 10% fetal bovine serum at 37 °C and 5% CO_2. Cell transfection was performed by electroporation with an Amaxa 4D-Nucleofector (Lonza GmbH) and the SF Cell Line 4D-Nucleofector X Kit (Lonza GmbH) using 80–90% confluent cells after dissociation by trypsinization. For each experiment (n = 1) shown in Figures 1 and 2, 1.8 × 10^6 cells were mixed with 0.6 µg of pcDNA3.1(-) bearing one of the tested Or47a constructs (or empty vector), and 0.6 µg of pcDNA3.1(-) bearing Orco (or empty vector), and then loaded in an electroporation cuvette (total of 1.2 µg/cuvette plasmid DNA). For experiments shown in Figure 2 with the pDmelOR-R.E.hOr47a construct, 0.8 µg of plasmid per cuvette was used (total of 0.8 µg/cuvette plasmid DNA). For each experiment (n = 1) shown in Figure 3, 2 cuvettes with ~1.1 × 10^6cells/cuvette were mixed with 0.8 µg/cuvette of pDmelOR-R.E.hOr47a, or 2 cuvettes with ~0.67 × 10^6 cells/cuvette were transfected with 0.8 µg/cuvette of pDmelOR-R.E.hOr56a; for control experiments with the pCMV-BI plasmid, 2 cuvettes with ~1 × 10^6 cells/cuvette were transfected with 0.8 µg/cuvette of pCMV-BI. Electroporated cells were cultured on poly-l-lysine (0.01%, Sigma-Aldrich) coated coverslips at ~3 × 10^5cells/well (6 wells per cuvette) in a 24-well plate (for experiments shown in Figures 1 and 2), or they were split into 48 wells in Poly-D-Lysine Cellware 96-well black/clear plate (BD Biosciences, Cat. Nr. 354640) (for experiments shown in Figure 3), with a 1:1 mixture of DMEM zero Ca^{2+} (Gibco, Cat. Nr. 21068) supplemented with 1% Roti-Cell glutamine solution (Cat. Nr. 9183.1, Carl Roth), and F12 (Gibco, Cat. Nr. 21765) in a 1:1 mixture, supplemented with 10% fetal bovine serum. Zero Ca^{2+} DMEM was preferred to standard DMEM in a 1:1 mix with F12, as we previously showed that such low-Ca^{2+} culture medium better supports the functional expression of insect ORs in HEK293 cells (Miazzi et al. 2019).

Functional imaging

Cells were imaged 24 h postelectroporation. Cells were incubated in Opti-MEM medium (Cat. Nr. 31985, Gibco), containing 5 µM Fura-2 acetoxymethyl ester (Molecular Probes, Invitrogen) for 30 min at room temperature. After incubation, cells were washed 3 times and kept throughout the experiment in standard extracellular solution (SES) containing 135 mM NaCl, 5 mM KCl, 1 mM $CaCl_2$, 1 mM $MgCl_2$, 10 mM HEPES (4-(2-hydroxyethyl)-1-piperazineethanesulfonic acid), 10 mM glucose (pH = 7.4; osmolarity = 295 mOsmol/L). Excitation with 340 and 380 nm light for 150 ms per frame was obtained using a monochromator (Polychrome V, Till Photonics), coupled to an epifluorescence microscope (Axioskop FS, Zeiss) by means of a water immersion objective (LUMPFL40×W/IR/0.8; Olympus) and controlled by an imaging control unit (ICU, Till Photonics). Emitted light was separated by a 400 nm dichroic mirror, filtered with a 420 nm long-pass filter and acquired by a cooled CCD camera (Sensicam, PCO Imaging) controlled by the TILLVision 4.5 software (TILL Photonics). The final image resolution was 640 × 480 pixels in a frame of 175 × 130 µm. Experiments lasted 10 min with a sampling interval of 5 s. Stimuli consisting of 100 µL of pentyl acetate and VUAA1 solutions (100 µM in SES) were delivered via pipette in proximity of the objective at 50 and 350 s, respectively. Movies of the imaging recordings were exported as uncompressed TIFF files from the TILLVision software and analyzed using custom scripts for Fiji ImageJ2.0 (Schindelin et al. 2012; Rueden et al. 2017) (see Supplementary Code). Briefly, the free intracellular Ca^{2+} concentration ($[Ca^{2+}]_i$) was calculated after correcting for background, flat-field and movement (performed using the image stabilizer plugin for ImageJ—http://www.cs.cmu.edu/~kangli/code/Image_Stabilizer.html) artifacts. $[Ca^{2+}]_i$ was calculated according to the equation:

$$\left[Ca^{2+}\right]_i = K_{eff}\frac{R - R_{min}}{R_{max} - R}$$

Where K_{eff} = 1747 nM, R_{min} = 0.1, and R_{max} = 5.1. Calcium calibration was performed using the Fura-2 calcium calibration kit (Cat. Nr. F6774, Invitrogen). Cells were identified as regions of interest (ROI) using the free-hand selection tool of Fiji ImageJ2.0 and the mean $[Ca^{2+}]_i$ of each ROI for each time point was calculated and used for subsequent analysis. Data analysis was performed using custom scripts in R (see Supplementary Code). Briefly, cells with a basal mean $[Ca^{2+}]_i$ level higher than 200 nM before pentyl acetate application (0 ≤ Time (s) ≤ 40) or with a $[Ca^{2+}]_i$ standard deviation > 10 nM before pentyl acetate or VUAA1 application (0 ≤ Time (s) ≤ 40 and 300 ≤ Time (s) ≤ 340, respectively) were excluded from further analysis. Variations of the intracellular Ca^{2+} concentration ($\Delta[Ca^{2+}]_i$) were calculated from the base level before pentyl acetate application for all analyzed cells; imaged cells coming from the same electroporation experiment (and imaged from up to 6 wells) were averaged in order to calculate the experimental time series and the responses following stimuli application. Calculated responses to stimuli were normalized to the $[Ca^{2+}]_i$ before each stimulus application. Statistical analysis was performed using parametric or nonparametric tests (according to the data distribution) and P-values were corrected for multiple comparisons using Holm's correction. Software plugin and packages used are listed in the Supplementary Table 2.

Imaging experiments using an automated platform were performed on a BD Pathway 855 (BD Biosciences) controlled by the AttoVision software (version 1.6/855). Excitation at 340 (for 150 ms) and 380 nm (for 250 ms) was performed using the BD Pathway 855 settings and filters for Fura-2 with a 5 s interval between frames. Stimuli consisted of 20 µL solutions of odor at the desired concentration (Figure 3), or 20 µL of 100 µM VUAA1 in SES. The odor solution was presented at the 10th frame, while the VUAA1 solution was presented at the 30th frame. After background subtraction, cells were segmented using the built-in tools of AttoVision and mean ROI intensity values were exported as text files for subsequent analysis

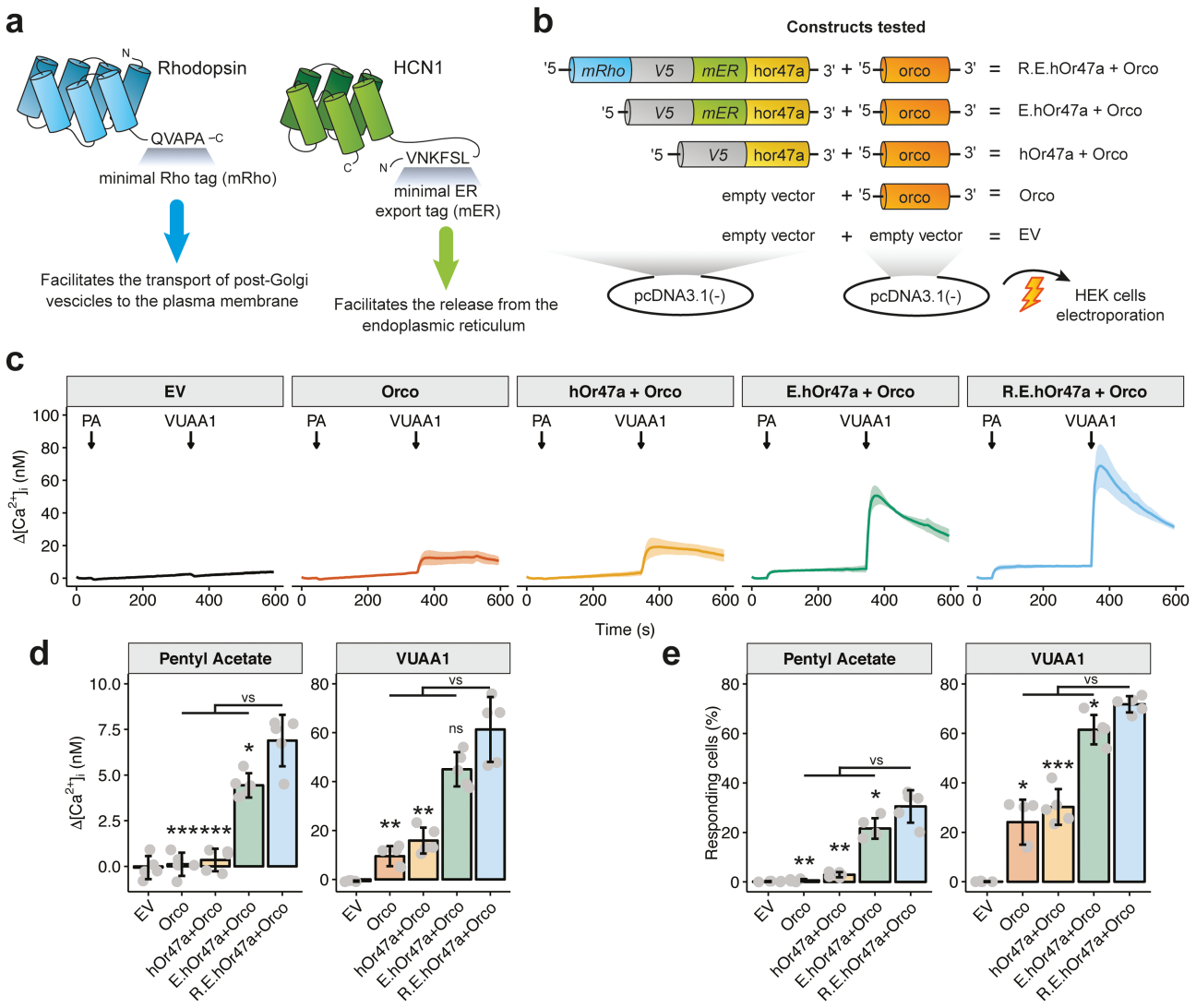

Figure 1. Optimization of OR trafficking to the plasma membrane in HEK293 cells. (**a**) The human HCN1 receptor sequence ^{106}VNKFSL^{111} encoding a minimal endoplasmic reticulum release signal ("mER", or "E") and the human Rhodopsin sequence ^{344}QVAPA^{348} encoding a minimal Rho tag ("mRho", or "R") were used to enhance the functional expression of insect ORs by promoting their exit from the endoplasmic reticulum and the transport of post-Golgi vesicles to the plasma membrane, respectively. (**b**) Schematic representation of the constructs tested. HEK293 cells were cotransfected by electroporation with 2 pcDNA3.1(-) plasmid constructs. The first, with the insertion of a human codon-optimized version of the *D. melanogaster* Or47a (hOr47a) tagged at the N-terminus with: a peptide composed of the mRho, mER and a V5 tag—to detect the receptor via immunochemistry if necessary—(R.E.hOr47a construct), or tagged only with the mER and V5 peptides (E.hOr47a) or the V5 tag alone (hOr47a). The second construct was constituted by a noncodon-optimized version of *D. melanogaster* Orco coreceptor. As controls, cells were cotransfected with the Orco coreceptor together with the empty vector backbone (EV) instead of the hOr47a construct, or with the empty vector alone. (**c**) Changes in intracellular calcium concentration over time ($\Delta[Ca^{2+}]_i$) in HEK293 cells transfected with the constructs shown in panel (b), following stimulations with 100 µL of 100 µM of the Or47a agonist pentyl acetate (PA) at 50 s and the synthetic Orco agonist VUAA1 at 350 s. Graphs represent mean ± SD. $n = 5$ for each panel. Each $n = 1$ represents the mean of all imaged cells coming from each independent electroporated cuvette (see Methods). (**d**) Intensity of calcium responses following a pentyl acetate or a VUAA1 stimulation in cells transfected with the constructs described in panel (b). Values were extracted 50 s after a stimulation with 100 µL of 100 µM pentyl acetate, and 20 s after a stimulation with 100 µL of 100 µM VUAA1. Mean ± SD values for pentyl acetate: EV, -0.07 ± 0.63; Orco, 0.11 ± 0.64; hOr47a + Orco, 0.35 ± 0.61; E.hOr47a + Orco, 4.44 ± 0.66; R.E.hOr47a + Orco, 6.89 ± 1.41. Statistical analysis for pentyl acetate: R.E.hOr47a + Orco versus E.hOr47a + Orco: $t = 3.52$, $P = 0.014$; R.E.hOr47a + Orco versus hOr47a + Orco: $t = 9.52$, $P < 0.001$; R.E.hOr47a + Orco versus Orco: $t = 9.81$, $P < 0.001$. Mean ± SD values for VUAA1: EV, –0.68 ± 0.24; Orco, 9.52 ± 4.11; hOr47a + Orco, 15.88 ± 5.29; E.hOr47a + Orco, 45.02 ± 7.02; R.E.hOr47a + Orco, 61.32 ± 13.29. Statistical analysis for VUAA1: R.E.hOr47a + Orco versus E.hOr47a + Orco: $t = 2.42$, $P = 0.051$; R.E.hOr47a + Orco versus hOr47a + Orco: $t = 7.10$, $P = 0.0015$; R.E.hOr47a + Orco versus Orco: $t = 8.32$, $P = 0.0015$. (**e**) Percentage of responding ROIs following a pentyl acetate or a VUAA1 stimulation. Mean ± SD values for pentyl acetate: EV, 0.18 ± 0.16; Orco, 0.64 ± 0.50; hOr47a + Orco, 2.90 ± 1.05; E.hOr47a + Orco, 21.61 ± 4.16; R.E.hOr47a + Orco, 30.51 ± 6.56. Statistical analysis for pentyl acetate: R.E.hOr47a + Orco versus E.hOr47a + Orco: $t = 2.56$, $P = 0.039$; R.E.hOr47a + Orco versus hOr47a + Orco: $t = 9.29$, $P = 0.0015$; R.E.hOr47a + Orco versus Orco: $t = 10.16$, $P = 0.0015$. Mean ± SD values for VUAA1: EV, 0.06 ± 0.14; Orco, 24.12 ± 9.10; hOr47a + Orco, 30.24 ± 7.21; E.hOr47a + Orco, 61.49± 5.95; R.E.hOr47a + Orco, 71.76 ± 3.29. Statistical analysis for VUAA1: R.E.hOr47a + Orco versus E.hOr47a + Orco: $t = 3.38$, $P = 0.015$; R.E.hOr47a + Orco versus hOr47a + Orco: $t = 11.71$, $P < 0.001$; R.E.hOr47a + Orco versus Orco: $W = 25$, $P = 0.016$ (Wilcoxon rank test). Unless otherwise stated, tests are unpaired 2-tail Welch's *t*-test. *P* values corrected for multiple comparisons using Holm's correction. Bar plots represent mean ± SD, $n = 5$ for each treatment. $^*P < 0.05$, $^{**}P < 0.01$, $^{***}P < 0.001$, ns = not significant.

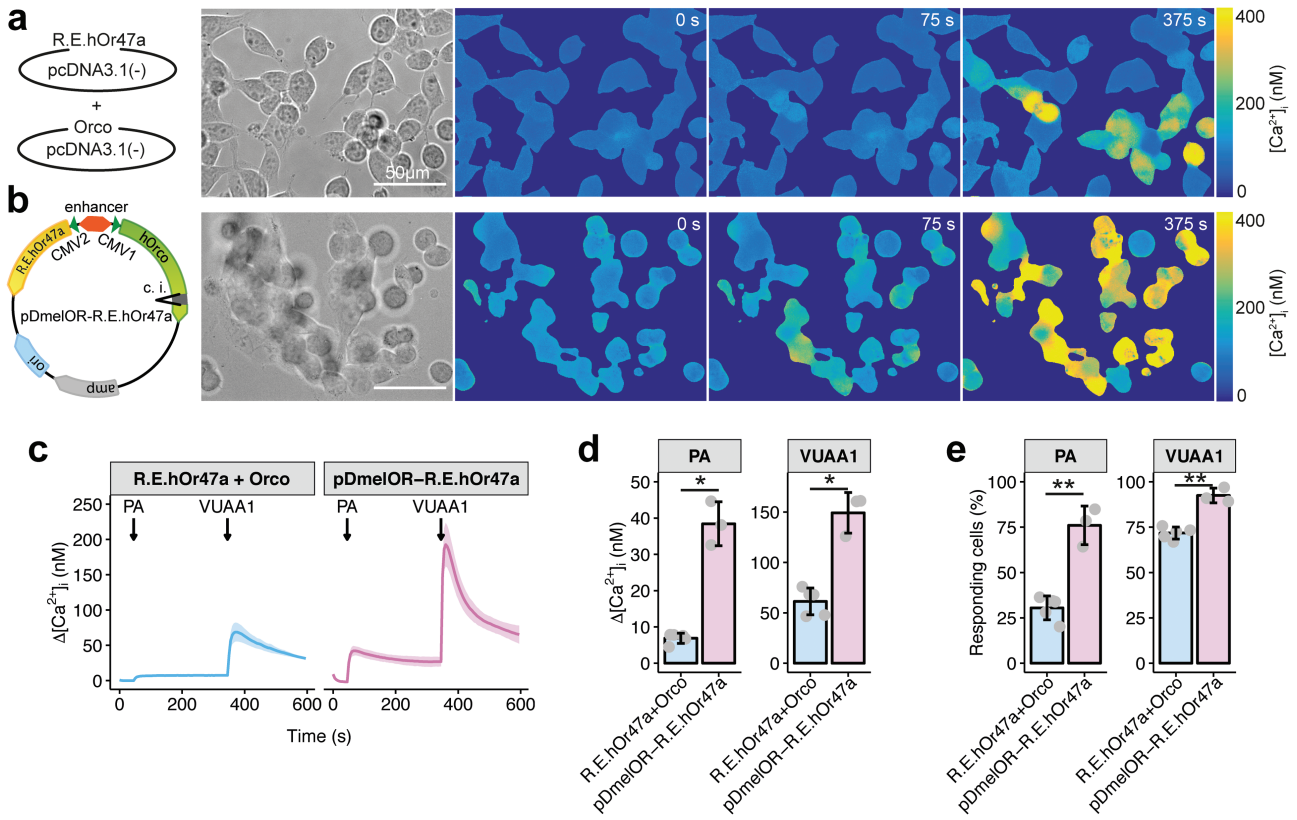

Figure 2. OR cotransfection via a bidirectional expression vector in HEK293 cells. (**a,b**) Examples of calcium imaging experiments with HEK293 cells cotransfected with the R.E.hOr47a + Orco constructs in 2 different pcDNA3.1(-) vectors (a) and with the pDmelOR-R.E.hOr47a housing both the hOr47a and a codon-optimized version of Orco (hOrco) bearing the β-globin/IgG chimeric intron (c.i.) (b). Panels represent—from left to right—a schematic representation of the constructs tested; transmission light image of the tested HEK293 cells; base level $[Ca^{2+}]_i$ of transfected HEK293 cells (0 s); $[Ca^{2+}]_i$ 25 s after application of 100 µL of 100 µM pentyl acetate (75 s) and 25 s after application of 100 µL of 100 µM VUAA1 (375 s). Scale bar = 50 µm. (**c**) Changes in intracellular calcium concentration over time ($\Delta[Ca^{2+}]_i$) in HEK293 cells transfected with the construct shown in panels (a-b), following stimulations with 100 µL of 100 µM of the Or47a agonist pentyl acetate (PA) at 50 s and the synthetic Orco agonist VUAA1 at 350 s. Graphs represent mean ± SD. $n = 5$ for R.E.hOr47a + Orco and $n = 3$ for pDmelOR-R.E.hOr47a. Each $n = 1$ represents the mean of all imaged cells coming from independently electroporated cuvettes (see Methods). (**d**) Intensity of calcium responses following a pentyl acetate or a VUAA1 stimulation in cells transfected with the constructs described in panels (a–b). $\Delta[Ca^{2+}]_i$ values were extracted 50 s after a stimulation with 100 µL of 100 µM pentyl acetate, and 20 s after a stimulation with 100 µL of 100 µM VUAA1. Mean ± SD values for pentyl acetate: R.E.hOr47a + Orco, 6.89 ± 1.41; pDmelOR-R.E.hOr47a, 38.43 ± 6.04. Statistical analysis for pentyl acetate: pDmelOR-R.E.hOr47a versus R.E.hOr47a + Orco, $t = 8.90$, $P = 0.010$, Two-tailed Welch's t test. Mean ± SD values for VUAA1: R.E.hOr47a + Orco, 61.32 ± 13.29; pDmelOR-R.E.hOr47a, 149.24 ± 20.12. Statistical analysis for VUAA1: pDmelOR-R.E.hOr47a versus R.E.hOr47a + Orco, W = 15, $P = 0.036$, Wilcoxon rank sum test. Graphs represent mean ± SD. $n = 5$ for R.E.hOr47a + Orco and $n = 3$ for pDmelOR-R.E.hOr47a. (**e**) Percentage of responding ROIs following a pentyl acetate or a VUAA1 stimulation. Mean ± SD values for pentyl acetate: R.E.hOr47a + Orco, 30.51 ± 6.56; pDmelOR-R.E.hOr47a, 76.01± 10.64. Statistical analysis for pentyl acetate: pDmelOR-R.E.hOr47a versus R.E.hOr47a + Orco: $t = 6.68$, $P = 0.0073$. Mean ± SD values for VUAA1: R.E.hOr47a + Orco, 71.76 ± 3.29; pDmelOR-R.E.hOr47a, 92.47± 4.03. Statistical analysis for VUAA1: pDmelOR-R.E.hOr47a versus R.E.hOr47a + Orco: $t = 7.52$, $P = 0.0024$. Two-tailed Welch's t tests. Graphs represent mean ± SD. $n = 5$ for R.E.hOr47a + Orco and $n = 3$ for pDmelOR-R.E.hOr47a.

in R (see Supplementary Code). Briefly, for experiments shown in Figure 3d–h, ROIs showing high base level fluorescence standard deviation (> 0.05 × R [340/380 nm] ratio) or a high intracellular Ca^{2+} (> 2 × R [340/380 nm] ratio) in frames 1–9 (before odor stimulus application), or showing no or very small VUAA1 responses (local max after VUAA1 application < 1.5 × baselevel R [340/380 nm] ratio) or showing an increasing monotonic VUAA1 response (i.e., no peak in the VUAA1 response before the end of the experiment) were excluded from analysis. For control experiments (Figure 3i), only ROIs with high base level fluorescence standard deviation, or with high intracellular Ca^{2+} before odor stimulus application were deleted. ROIs from wells subjected to the same treatment within the same plate were averaged ($n = 1$) in order to calculate the experimental time series and the responses following stimuli application. Statistical analysis was performed using parametric or nonparametric tests (according to the data distribution) and P-values were corrected for multiple comparisons using Dunnett's correction. Software plugin and packages used are listed in the Supplementary Table 2.

OR agonists

The following odors and agonists were used: pentyl acetate (Sigma-Aldrich, Cat. Nr. 109584, 99%), butyl acetate (Fluka, Cat. Nr. 45860, ≥99.5% (GC), ACS Reagent), methyl hexanoate (Fluka, Cat. Nr. 21599, 99.8%, analytical standard grade), propyl acetate (Sigma-Aldrich, Cat. Nr. 133108, 99%; Fluka, Cat. Nr. 40858, ≥99%, analytical standard grade), 3-methylthio-1-propanol (Sigma-Aldrich, Cat. Nr. 318396, 98%; Sigma-Aldrich, Cat. Nr. W341509, ≥98% synthetic, FG grade), hexyl acetate (Sigma-Aldrich, Cat. Nr. 108154, 99%), isobutyl acetate (Fluka, Cat. Nr. 94823, 99.8%, analytical standard grade), 2-heptanone (Sigma-Aldrich, Cat. Nr. W254401, 98% synthetic, FG grade), 3-octanol (Sigma-Aldrich, Cat. Nr. 218405,

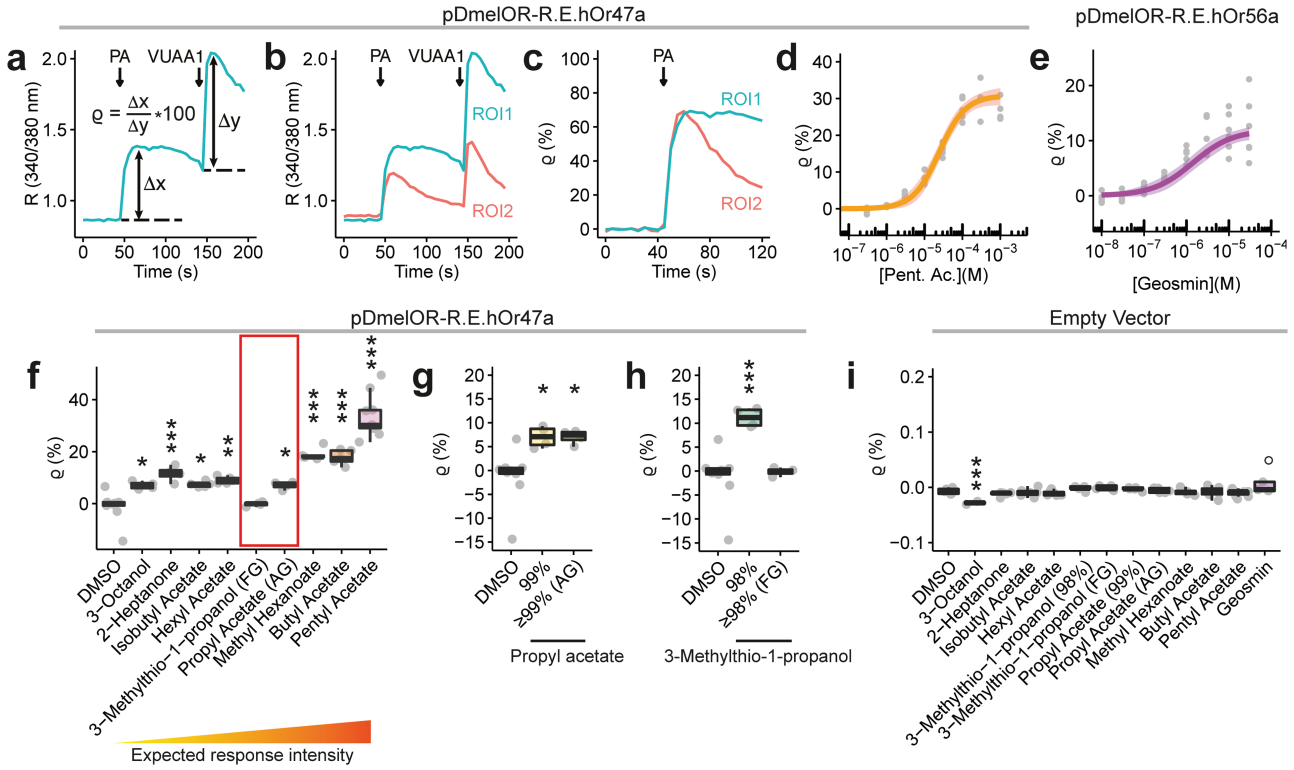

Figure 3. Analysis of insect OR agonist sensitivity and specificity by means of an automated imaging platform. (**a**) Normalization of the odor response respect to the VUAA1 internal control. After calculating the ratio (R) between the emission light at 340 nm and 380 nm, base levels were subtracted from peak agonist responses to obtain the odor, e.g., pentyl acetate (PA), and the VUAA1 net responses (Δx and Δy, respectively). The ratio ϱ (*rho*) between the odor and VUAA1 net responses expressed in percentage ($\varrho = [\Delta x/\Delta y]*100$) can be used to account for the cell-specific OR expression level due to the transient transfection protocol. (**b,c**) Example showing how normalization of the odor response to the VUAA1 internal control can reduce response variability. (b) Time series of R (340/380 nm) ratios for 2 regions of interests (ROI1 and ROI2) showing different response intensities to the same odor and VUAA1 stimulation. (c) Time series of normalized ϱ values for the odor responses of the same ROI1 and ROI2 as shown in panel (b). ϱ values reveal that both ROI1 and ROI2 show a very similar maximal response to the PA stimulation. (**d,e**) Dose–response curve for HEK293 cells transfected with pDmelOR-R.E.hOr47a and stimulated with pentyl acetate (d), or with pDmelOR-R.E.hOr56a and stimulated with geosmin (e). Data were fitted to a 3-parameter logistic function using the drc package in R (see Supplementary Code). Values of the data fit (mean ± st. error) for pDmelOR-R.E.hOr47a: slope, –2.89 ± 0.42; upper limit, 30.80 ± 1.28; EC_{50} (log), –4.61 ± 0.06. EC_{50} values expressed in Molar (estimate, 2.5% and 97.5% confidence intervals): $2.45{\cdot}10^{-5}$ (1.83×10^{-5}; 3.29×10^{-5}). Values of the data fit for pDmelOR-R.E.hOr56a: slope, –2.46 ± 0.58; upper limit, 11.93 ± 0.92; EC_{50} (log), –6.14 ± 0.13. EC_{50} values expressed in Molar (estimate, 2.5% and 97.5% confidence intervals): $7.19{\cdot}10^{-7}$ (3.97×10^{-7}; 1.30×10^{-6}). Plot shows estimate ± SE. For $5 \le n \le 6$ (b) and $n = 7$ (c) for each odor concentration. (**f**) Odor response profile for Or47a using the pDmelOR-R.E.hOr47a construct. Odors are disposed according to their expected potency as agonists according to the DoOR database (see Supplementary Figure 2). Kruskall-Wallis rank sum test: $\chi^2 = 50.148$, df = 9, $P < 0.001$. Post-hoc Dunnett's test for comparing each treatment versus DMSO. 3-octanol versus DMSO, $P = 0.039$; 2-heptanone versus DMSO, $P < 0.001$; isobutyl acetate versus DMSO, $P = 0.013$; hexyl acetate versus DMSO, $P = 0.002$; 3-methylthio-1-propanol (FG) versus DMSO, $P = 1$; propyl acetate (AG) versus DMSO, $P = 0.036$; methyl hexanoate versus DMSO, $P < 0.001$; butyl hexanoate versus DMSO, $P < 0.001$; pentyl acetate versus DMSO, $P < 0.001$. $4 \le n \le 10$. The red box highlights 2 odors whose response intensities do not follow the expected trend, i.e., 3-methilthio-1-propanol and pentyl acetate. (**g**) The effect of propyl acetate is consistent across commercial stocks with different purity. The response to pentyl acetate was significant compared to the DMSO control when working solutions were prepared from a 99% purity stock odor (Sigma-Aldrich, Cat. Nr. 133108), and a ≥99% analytical standard grade (AG) stock odor (Fluka, Cat. Nr. 40858). Kruskall–Wallis rank sum test: $\chi^2 = 10.088$, df = 2, $P = 0.0064$. Post-hoc Dunnett's test for comparing each treatment versus DMSO. 99% versus DMSO, $P = 0.0147$; ≥99% AG versus DMSO, $P = 0.0147$. $4 \le n \le 9$. (**h**) The effect of 3-methilthio-1-propanol is not consistent across commercial stocks with different purity. Responses were significant compared to the DMSO control when working solutions were prepared from a 98% purity stock odor (Sigma-Aldrich, Cat. Nr. 318396), but not from a ≥98% food/pharmaceutical (FG) grade stock odor (Sigma-Aldrich, Cat. Nr. W341509). Kruskall–Wallis rank sum test: $\chi^2 = 8.681$, df = 2, $P = 0.013$. Post-hoc Dunnett's test for comparing each treatment versus DMSO. 98% versus DMSO, $P = 0.904$; ≥98% (FG) versus DMSO: $P < 0.001$. $4 \le n \le 9$. (**i**) Responses of HEK293 cells transfected with the pCMV-BI empty vector to odor stimuli (300 µM for all odors, except 30 µM for geosmin) and DMSO. Kruskall–Wallis rank sum test: $\chi^2 = 27.115$, df = 12, $P = 0.0074$. Post-hoc Dunnett's test for comparing each treatment versus DMSO. 3-octanol versus DMSO, $P = 0.00064$; 2-heptanone versus DMSO, $P = 0.734$; isobutyl acetate versus DMSO, $P = 0.996$; hexyl acetate versus DMSO, $P = 0.949$; 3-methylthio-1-propanol (98%) versus DMSO, $P = 0.762$; 3-methylthio-1-propanol (FG) versus DMSO, $P = 0.572$; propyl acetate (99%) versus DMSO, $P = 0.922$; propyl acetate (AG) versus DMSO, $P > 0.999$; methyl hexanoate versus DMSO, $P > 0.999$; butyl acetate versus DMSO, $P > 0.999$; pentyl acetate versus DMSO, $P = 0.961$; geosmin versus DMSO, $P = 0.749$. For geosmin, one data point (black circle in the bar plot) was considered as an outlier and was omitted from analysis. $2 \le n \le 11$. $^{***}P < 0.001$, $^{**}P < 0.01$, $^{*}P < 0.05$.

99%), (±)-geosmin (Sigma-Adrich, Cat. Nr. UC18, ≥98% [GC]), VUAA1 (CAS Nr. 525582-84-7) was synthesized by the group "Mass Spectrometry/Proteomics" of the Max Planck Institute for Chemical Ecology (Jena, Germany). Stimuli stocks consisted of 100 mM solutions in dimethyl sulfoxide (DMSO, Sigma-Aldrich, Cat. Nr. D8418); working solutions were prepared fresh diluting 100 mM stocks in SES to the desired concentration just before the start of the experiment. Negative controls consisted of the equivalent maximum volume of DMSO used to prepare odor stimuli solutions diluted in SES.

Results

Targeting of insect ORs to the plasma membrane

We first tested whether the ^{344}QVAPA^{348} (minimal Rho tag, abbreviated as "mRho" or "R" tag) and the ^{106}VNKFSL^{111} (minimal ER export tag, abbreviated as "mER" or "E" tag) peptides from the human Rhodopsin and the HCN1 channel, respectively (Figure 1a) could improve the intracellular trafficking of hOr47a to the plasma membrane in mammalian cells.

For this purpose, we performed functional imaging experiments on HEK293 cells transiently transfected with the constructs shown in Figure 1b and loaded with the calcium dye Fura-2. We stimulated the hOr47a/Orco heteromers with the Or47a agonist pentyl acetate and the Orco synthetic agonist VUAA1 (Figure 1c). We quantified the increase in intracellular free calcium with respect to the base level ($\Delta[Ca^{2+}]_i$ (nM)) (Figure 1d) and the distribution of Ca^{2+} responses (Figure 1e and Supplementary Figure 1) for each tested construct (i.e., treatment), in order to compare the number of excited cells after presentation of the odor pentyl acetate and the Orco agonist VUAA1.

HEK293 cells cotransfected with the R.E.hOr47a and Orco constructs showed significantly higher calcium responses after stimulation with 100 µM pentyl acetate and 100 µM VUAA1, compared to cells transfected with an untagged version of hOr47a (Figure 1d). Moreover, the R.E.hOr47a construct induced significantly higher calcium responses to pentyl acetate than the E.hOr47a construct bearing the mER tag alone (Figure 1d, left panel). In order to calculate and compare the number of responding cells between the tested treatments, we used the distribution of Ca^{2+} responses from HEK293 cells transfected with the empty pcDNA3.1(-) vector to calculate threshold values to classify cells as "responding" or "nonresponding" to an OR agonist. To do so, we calculated the mean response intensity + 2 × SD ($\Delta[Ca^{2+}]_i$, in nM) of the top (most responsive) 0.5 percentile of the cumulative distribution of analyzed control cells (transfected with empty vector) after a pentyl acetate and VUAA1 stimulation. The resulting threshold values were 6.75 nM for pentyl acetate and 6.25 nM for VUAA1 (Supplementary Figure 1). Only 2.9 ± 1.05% (mean ± SD) of cells transfected with hOr47a/Orco showed a $\Delta[Ca^{2+}]_i \geq 6.75$ nM after a 100 µM pentyl acetate stimulation, while 21.61 ± 4.16% of cells transfected with E.hOr47a/Orco and 30.51 ± 6.56% of cells transfected with R.E.hOr47a/Orco reached such threshold. When comparing cell responses after a 100 µM VUAA1 stimulation, only 30.24 ± 7.21% of cells transfected with hOr47a/Orco showed an $\Delta[Ca^{2+}]_i \geq 6.25$ nM, while 61.49 ± 5.95% and 71.76 ± 3.29% of cells transfected with E.hOr47a/Orco and R.E.hOr47a/Orco, respectively could be defined as "responding" (Figure 1e and Supplementary Figure 1). These results show that the mRho and mER tags can significantly enhance the intensity of the Ca^{2+} response and the number of responding units in functional imaging experiments with insect OR transfected cells. Moreover, they show that the addition of mRho has a significant positive effect compared to the mER tag alone.

Optimization of OR cotransfection in mammalian cells

Although vectors with 2 expression cassettes disposed in series have already been used successfully (Bohbot et al. 2011), we designed a new vector bearing a bidirectional expression cassette to improve the chances of successful cotransfection for a tuning OR and the coreceptor Orco. The rationale for this choice was to minimize the size of the empty vector backbone, by flanking a single CMV enhancer with 2 minimal CMV promoters. The vector consisted of the pCMVTNT plasmid backbone (including the *amp* resistance gene and a high-copy number *ori*) and the bidirectional expression cassette of the pBI-CMV1 vector, in order to guide the expression of 2 genes simultaneously (see Methods). We first inserted a human codon-optimized version of *D. melanogaster* Orco (hOrco) tagged at the N-terminus with a myc tag in correspondence of the multiple cloning site 1 of the vector. As the CMV promoter can initiate expression in *Escherichia coli* (Lewin et al. 2005) and Orco forms leaky ion channels, the unintended expression of Orco during cloning may reduce the viability of successfully transformed bacterial colonies. To avoid such inconvenience, we inserted a β-globin/IgG chimeric intron within the Orco sixth transmembrane domain. In this way, only mammalian cells can splice out the intron, leading to the production of functional Orco ion channels. The resulting plasmid, named pDmelOR, is intended to serve as a plasmid backbone to insert one of the 61 (including splice variants) tuning ORs of *D. melanogaster* (Robertson et al. 2003), and the same principle can be adapted to optimize the functional expression of ORs belonging to any insect species.

In order to evaluate the performance of the bidirectional pDmelOR vector against a standard cotransfection protocol, we compared the response profile of HEK293 cells transfected with pDmelOR-R.E.hOr47a to that of cells cotransfected with an Orco and an R.E.hOr47a construct inserted in a pcDNA3.1(-) each (Figure 2a–c). HEK293 cells transfected with pDmelOR-R.E.hOr47a showed a significantly higher $\Delta[Ca^{2+}]_i$ in response to both pentyl acetate and VUAA1 stimulation, with respect to cells cotransfected with R.E.hOr47a and Orco in pcDNA3.1(-) (Figure 2d). Moreover, a significantly higher number of cells responded to pentyl acetate and after transfection with pDmelOR-R.E.hOr47a compared to cells cotransfected with R.E.hOr47a and Orco in pcDNA3.1(-) (Figure 2e). These results propose the pDmelOR vector as an efficient transfection tool for the expression of insect OR fusion constructs with higher efficacy than standard plasmid cotransfection procedures.

Optimization of transient transfection for automated imaging platforms

Finally, we took advantage of the high level of functional expression reached combining the increased OR trafficking to the plasma membrane using the mRho and mER tags, together with the optimization of the transfection protocol due to the pDmelOR vector, to validate our method using an automated imaging platform (Figure 3).

A monoclonal stable cell line guarantees a highly homogeneous level of transgene expression within the cell population, which minimizes variability in functional assays. On the other hand, the expected variability in a population of transiently transfected cells is much higher, due to the variation in plasmid copy number between cells that results in different levels of functional expression of the gene of interest. To control for this phenomenon, we stimulated tested cells with VUAA1 100 s after the presentation of the odor stimulus, in order to use the intensity of the response to this synthetic OR agonist as a proxy of the OrX/Orco functional expression level for each cell. In this way, we could remove from downstream analyses those cells that were not expressing ORs at sufficient levels (see Methods), and we could normalize the odor response for each cell to the intensity of the VUAA1 response, thus minimizing the variability induced by the transient transfection protocol (Figure 3a–c).

Using this method, we built dose–response curves for 2 *D. melanogaster* ORs, namely the broadly tuned receptor Or47a and the narrowly tuned Or56a, stimulated with their main agonists,

pentyl acetate and geosmin, respectively, and in both cases, the data could be used to obtain high quality fits (Figure 3d–e). We then tested whether the tuning properties for the Or47a receptor reported in the DoOR database (Münch and Galizia 2016) could be replicated in HEK293 cells. To do so, we selected 9 odors among the known most potent agonists for Or47a (Supplementary Figure 2) and assessed their relative potency using our assay (Figure 3f). Interestingly, when ranked according to their expected potency, compared to the DMSO negative control, the odor agonists did not show a monotonic increasing pattern. Odor properties as solubility in water-based solutions may play a role in explaining such pattern. Moreover in the case of 3-octanol, the odor application significantly affected cell activity independently of Or47a expression, as cells transfected with the negative control plasmid showed a significant reduction in the cell fluorescence base level (Figure 3i). However, we further investigated whether odor purity could have influenced our results. To do so, we tested 2 odors (propyl acetate and 3-methylthio-1-propanol) whose relative potency differed from the expected pattern (compare Figure 3f with Supplementary Figure 2). For each odor, we tested 2 aliquots with different chemical grade. Interestingly, while the responses to propyl acetate were not affected by the odor chemical grade (Figure 3g), the responses to 3-methylthio-1-propanol were significantly affected by this factor, indicating that 3-methylthio-1-propanol might not be an actual agonist of Or47a and the source of OR activation might originate from impurities within the extract (Figure 3h).

Discussion

Functional expression in heterologous systems represents a key method to elucidate the function and structure of membrane protein. When confronted with the choice of which expression system to use, there are several factors to consider: from the codon usage of the gene of interest and necessary post-translational modifications (Gomes et al. 2016), to the type of downstream applications and the level of automation required. HEK293 cells represent a well-understood and very versatile choice: their transcriptome has been extensively profiled (Sultan et al. 2008; Richard et al. 2010) providing fundamental information regarding possible cross-talk between heterologous and native proteins. Furthermore, an extensive set of molecular tools has already been optimized to support protein functional expression (for an overview, see Baser and van den Heuvel 2016), and these tools are amenable to a vast array of downstream applications, from imaging to electrophysiology, that can be performed with automated and high-throughput systems (Mattiazzi Usaj et al. 2016; Obergrussberger et al. 2018).

On such a basis, we decided to implement a fast, inexpensive, and versatile method for the expression of insect ORs in HEK293 cells. In order to achieve this result, we here tackled 2 main problems: the poor surface localization of OR proteins in mammalian cells and the limits imposed by the cotransfection of 2 genes (Orco and an odor-binding receptor) to obtain functional odor-gated ion channels. In order to improve the surface localization of insect ORs, we prepared fusion constructs carrying at the N-terminus small epitopes from the human HCN1 (mER) and Rhodopsin (mRho) that are known to facilitate the release of membrane proteins from the ER and the targeting to the plasma membrane, respectively. Using this method, we obtained a nearly 20-fold increase in the mean response (Figure 1d) and a 10-fold increase in the number of cells responding (Figure 1e and Supplementary Figure 1) to odor stimulation. Although we did not quantify how the mRho and mER epitopes affected the abundance of OR proteins in the plasma membrane, a correlation between an increased amount of OR proteins that successfully reach the cell plasma membrane and the increase in the mean Ca^{2+} response and the number of responding units is the most parsimonious explanation. Then, by adopting a new high-copy number vector based on a bidirectional expression cassette (Figure 2), we significantly improved the expression efficiency of ORs, showing that three-quarters of cells were stimulated with an overall 100-fold increase in the mean $\Delta[Ca^{2+}]_i$ in response to an odor stimulation, when compared to a standard cotransfection protocol with ORs lacking the HCN1 and Rhodopsin-derived tags (Figures 1 and 2 and Supplementary Figure 1). Finally, thanks to the high expression level and the possibility to use synthetic Orco agonists as internal stimulus controls to account for intercell variability, we showed that such a system is amenable to be used with automated platforms (Figure 3) and can be consequently used for high-throughput screenings.

Although we proved the effectiveness of such a system for 2 *D. melanogaster* ORs with different properties—a broadly tuned receptor as Or47a and the narrowly tuned Or56a—it remains to be shown how generalizable such approach is. Mammalian ORs are affected by similar problems regarding an incorrect intracellular trafficking in heterologous expression systems. Although specific classes of proteins have been shown to support the trafficking of mammalian ORs in native olfactory neurons and in heterologous systems (Saito et al. 2004; Mainland and Matsunami 2012), conserved OR residues linked to in silico structural stability were shown to impact their functional expression (Ikegami et al. 2019); we cannot exclude that insect ORs are subject to similar structural constraints.

Taken together, our results show that by optimizing the intracellular trafficking and transfection conditions of insect ORs, it is possible via transient transfection to achieve expression levels in HEK293 cells that are comparable to more time and resource-demanding methods such as the establishment of mammalian stable cell lines. Hence, we hope that such method can advance the study of insect ORs structure and function even in nonmodel organisms.

Supplementary material

Supplementary data are available at *Chemical Senses* online.

Funding

This work was supported by the European Union's Horizon 2020 research and innovation program under the Grant Agreement No. 662629 (F.M. and S.L.L.) and the Max Planck Society (D.W., S.S., M.K., and B.S.H.).

Acknowledgments

The authors thank Sabine Kaltofen for help in culturing and transfecting HEK293 cells, Sascha Buchs for help with the BD Pathway 855 setup, Kerstin Weniger and Anna Späthe with chemical profile analysis, Aleš Svatoš and Jerrit Weißflog for the synthesis of VUAA1 and Domenica Schnabelrauch for the in-house Sanger sequencing. The authors thank Antonella di Pizio (Leibniz-Institute for Food Systems Biology at the Technical University of Munich, Germany) for fruitful discussion.

Author contributions

F.M. and S.L.L. designed the study; D.W. and B.S.H. contributed to the study design; S.S., M.K., and B.S.H. obtained funding for the project; F.M. and C.H. created the constructs; F.M. performed the imaging experiments, analyzed the data, and wrote the first draft of the manuscript. All authors contributed to the final version of the manuscript.

Conflict of Interest

The authors declare no competing interests.

References

Ammon C, Schäfer J, Kreuzer OJ, Meyerhof W. 2002. Presence of a plasma membrane targeting sequence in the amino-terminal region of the rat somatostatin receptor 3. *Arch Physiol Biochem*. 110:137–145.

Baser B, van den Heuvel J. 2016. Assembling multi-subunit complexes using mammalian expression. In: Vega MC, editor. *Advanced technologies for protein complex production and characterization*. Cham: Springer International Publishing. p. 225–238.

Benton R, Sachse S, Michnick SW, Vosshall LB. 2006. Atypical membrane topology and heteromeric function of *Drosophila* odorant receptors in vivo. *PLoS Biol*. 4:e20.

Bohbot JD, Jones PL, Wang G, Pitts RJ, Pask GM, Zwiebel LJ. 2011. Conservation of indole responsive odorant receptors in mosquitoes reveals an ancient olfactory trait. *Chem Senses*. 36:149–160.

Butterwick JA, Del Mármol J, Kim KH, Kahlson MA, Rogow JA, Walz T, Ruta V. 2018. Cryo-EM structure of the insect olfactory receptor Orco. *Nature*. 560:447–452.

Corcoran JA, Jordan MD, Carraher C, Newcomb RD. 2014. A novel method to study insect olfactory receptor function using HEK293 cells. *Insect Biochem Mol Biol*. 54:22–32.

Deretic D, Williams AH, Ransom N, Morel V, Hargrave PA, Arendt A. 2005. Rhodopsin C terminus, the site of mutations causing retinal disease, regulates trafficking by binding to ADP-ribosylation factor 4 (ARF4). *Proc Natl Acad Sci USA* 102:3301–3306.

Dobritsa AA, van der Goes van Naters W, Warr CG, Steinbrecht RA, Carlson JR. 2003. Integrating the molecular and cellular basis of odor coding in the *Drosophila* antenna. *Neuron*. 37:827–841.

Fleischer J, Pregitzer P, Breer H, Krieger J. 2018. Access to the odor world: olfactory receptors and their role for signal transduction in insects. *Cell Mol Life Sci*. 75:485–508.

German PF, van der Poel S, Carraher C, Kralicek AV, Newcomb RD. 2013. Insights into subunit interactions within the insect olfactory receptor complex using FRET. *Insect Biochem Mol Biol*. 43:138–145.

Gomes AR, Byregowda SM, Veeregowda BM, Balamurugan V. 2016. An overview of heterologous expression host systems for the production of recombinant proteins. *Adv Animal and Veterinary Sci*. 4:346–356.

Gonzalez F, Witzgall P, Walker WBI. 2016. Protocol for heterologous expression of insect odourant receptors in *Drosophila*. *Front Ecol Evol*. 4:24.

Grosse-Wilde E, Svatos A, Krieger J. 2006. A pheromone-binding protein mediates the bombykol-induced activation of a pheromone receptor in vitro. *Chem Senses*. 31:547–555.

Hallem EA, Carlson JR. 2006. Coding of odors by a receptor repertoire. *Cell*. 125:143–160.

Halty-deLeon L, Miazzi F, Kaltofen S, Hansson BS, Wicher D. 2016. The mouse receptor transporting protein RTP1S and the fly SNMP1 support the functional expression of the *Drosophila* odorant coreceptor Orco in mammalian culture cells. *J Neurosci Methods*. 271:149–153.

Ikegami K, de March, CA, Nagai MH, Ghosh S, Do M, Sharma R, Bruguera ES, Lu YE, Fukutani Y, Vaidehi N, et al. 2019. Divergence from conserved residues underlies intracellular retention of mammalian odorant receptors. *BioRxiv*. doi:10.1101/605337.

Jones WD, Nguyen TA, Kloss B, Lee KJ, Vosshall LB. 2005. Functional conservation of an insect odorant receptor gene across 250 million years of evolution. *Curr Biol*. 15:R119–R121.

Jones PL, Pask GM, Rinker DC, Zwiebel LJ. 2011. Functional agonism of insect odorant receptor ion channels. *Proc Natl Acad Sci USA* 108:8821–8825.

Kiely A, Authier A, Kralicek AV, Warr CG, Newcomb RD. 2007. Functional analysis of a *Drosophila melanogaster* olfactory receptor expressed in Sf9 cells. *J Neurosci Methods*. 159:189–194.

Krieger J, Klink O, Mohl C, Raming K, Breer H. 2003. A candidate olfactory receptor subtype highly conserved across different insect orders. *J Comp Physiol A Neuroethol Sens Neural Behav Physiol*. 189:519–526.

Kurtovic A, Widmer A, Dickson BJ. 2007. A single class of olfactory neurons mediates behavioural responses to a *Drosophila* sex pheromone. *Nature*. 446:542–546.

Lewin A, Mayer M, Chusainow J, Jacob D, Appel B. 2005. Viral promoters can initiate expression of toxin genes introduced into *Escherichia coli*. *BMC Biotechnol*. 5:19.

Lodowski KH, Lee R, Ropelewski P, Nemet I, Tian G, Imanishi Y. 2013. Signals governing the trafficking and mistrafficking of a ciliary GPCR, rhodopsin. *J Neurosci*. 33:13621–13638.

Mainland J, Matsunami H. 2012. RAMP like proteins: RTP and REEP family of proteins. *Adv Exp Med Biol*. 744:75–86.

Mattiazzi Usaj M, Styles EB, Verster AJ, Friesen H, Boone C, Andrews BJ. 2016. High-content screening for quantitative cell biology. *Trends Cell Biol*. 26:598–611.

Mazelova J, Astuto-Gribble L, Inoue H, Tam BM, Schonteich E, Prekeris R, Moritz OL, Randazzo PA, Deretic D. 2009. Ciliary targeting motif VxPx directs assembly of a trafficking module through Arf4. *EMBO J*. 28:183–192.

Miazzi F, Schulze HC, Zhang L, Kaltofen S, Hansson BS, Wicher D. 2019. Low Ca2+ levels in the culture media support the heterologous expression of insect odorant receptor proteins in HEK cells. *J Neurosci Methods*. 312:122–125.

Mukunda L, Miazzi F, Kaltofen S, Hansson BS, Wicher D. 2014. Calmodulin modulates insect odorant receptor function. *Cell Calcium*. 55:191–199.

Münch D, Galizia CG. 2016. DoOR 2.0–comprehensive mapping of *Drosophila melanogaster* odorant responses. *Sci Rep*. 6:21841.

Nakagawa T, Sakurai T, Nishioka T, Touhara K. 2005. Insect sex-pheromone signals mediated by specific combinations of olfactory receptors. *Science*. 307:1638–1642.

Nakagawa T, Touhara K. 2013. Functional assays for insect olfactory receptors in *Xenopus* oocytes. In: Touhara K, (ed.). *Pheromone signaling*. Totowa (NJ): Humana Press. p. 107–119.

Neuhaus EM, Gisselmann G, Zhang W, Dooley R, Störtkuhl K, Hatt H. 2005. Odorant receptor heterodimerization in the olfactory system of *Drosophila melanogaster*. *Nat Neurosci*. 8:15–17.

Obergrussberger A, Goetze TA, Brinkwirth N, Becker N, Friis S, Rapedius M, Haarmann C, Rinke-Weiß I, Stölzle-Feix S, Brüggemann A, et al. 2018. An update on the advancing high-throughput screening techniques for patch clamp-based ion channel screens: implications for drug discovery. *Expert Opin Drug Discov*. 13:269–277.

Pan Y, Laird JG, Yamaguchi DM, Baker SA. 2015. An N-terminal ER export signal facilitates the plasma membrane targeting of HCN1 channels in photoreceptors. *Invest Ophthalmol Vis Sci*. 56:3514–3521.

Richard H, Schulz MH, Sultan M, Nürnberger A, Schrinner S, Balzereit D, Dagand E, Rasche A, Lehrach H, Vingron M, et al. 2010. Prediction of alternative isoforms from exon expression levels in RNA-Seq experiments. *Nucleic Acids Res*. 38:e112.

Robertson HM, Warr CG, Carlson JR. 2003. Molecular evolution of the insect chemoreceptor gene superfamily in *Drosophila melanogaster*. *Proc Natl Acad Sci USA* 100 (Suppl 2):14537–14542.

Rueden CT, Schindelin J, Hiner MC, DeZonia BE, Walter AE, Arena ET, Eliceiri KW. 2017. ImageJ2: ImageJ for the next generation of scientific image data. *BMC Bioinformatics*. 18:529.

Saito H, Kubota M, Roberts RW, Chi Q, Matsunami H. 2004. RTP family members induce functional expression of mammalian odorant receptors. *Cell*. 119:679–691.

Sato K, Pellegrino M, Nakagawa T, Nakagawa T, Vosshall LB, Touhara K. 2008. Insect olfactory receptors are heteromeric ligand-gated ion channels. *Nature*. 452:1002–1006.

Schindelin J, Arganda-Carreras I, Frise E, Kaynig V, Longair M, Pietzsch T, Preibisch S, Rueden C, Saalfeld S, Schmid B, et al. 2012. Fiji: an open-source platform for biological-image analysis. *Nat Methods*. 9:676–682.

Schülein R, Hermosilla R, Oksche A, Dehe M, Wiesner B, Krause G, Rosenthal W. 1998. A dileucine sequence and an upstream glutamate residue in the intracellular carboxyl terminus of the vasopressin V2 receptor are essential for cell surface transport in COS.M6 cells. *Mol Pharmacol*. 54:525–535.

Sultan M, Schulz MH, Richard H, Magen A, Klingenhoff A, Scherf M, Seifert M, Borodina T, Soldatov A, Parkhomchuk D, et al. 2008. A global view of gene activity and alternative splicing by deep sequencing of the human transcriptome. *Science*. 321:956–960.

Tai AW, Chuang JZ, Bode C, Wolfrum U, Sung CH. 1999. Rhodopsin's carboxy-terminal cytoplasmic tail acts as a membrane receptor for cytoplasmic dynein by binding to the dynein light chain Tctex-1. *Cell*. 97:877–887.

Touhara K, Vosshall LB. 2009. Sensing odorants and pheromones with chemosensory receptors. *Annu Rev Physiol*. 71:307–332.

Tsitoura P, Andronopoulou E, Tsikou D, Agalou A, Papakonstantinou MP, Kotzia GA, Labropoulou V, Swevers L, Georgoussi Z, Iatrou K. 2010. Expression and membrane topology of *Anopheles gambiae* odorant receptors in lepidopteran insect cells. *PLoS One*. 5:e15428.

Vosshall LB, Hansson BS. 2011. A unified nomenclature system for the insect olfactory coreceptor. *Chem Senses*. 36:497–498.

Wang G, Carey AF, Carlson JR, Zwiebel LJ. 2010. Molecular basis of odor coding in the malaria vector mosquito *Anopheles gambiae*. *Proc Natl Acad Sci USA* 107:4418–4423.

Wicher D, Schäfer R, Bauernfeind R, Stensmyr MC, Heller R, Heinemann SH, Hansson BS. 2008. *Drosophila* odorant receptors are both ligand-gated and cyclic-nucleotide-activated cation channels. *Nature*. 452:1007–1011.